PHYSICS

Hybrid cavity-antenna architecture for strong and tunable sideband-selective molecular Raman scattering enhancement

Ilan Shlesinger[1,2], Jente Vandersmissen[1], Eitan Oksenberg[1,3], Ewold Verhagen[1], A. Femius Koenderink[1,4]*

Plasmon resonances at the surface of metallic antennas allow for extreme enhancement of Raman scattering. Intrinsic to plasmonics, however, is that extreme field confinement lacks precise spectral control, which would hold great promise in shaping the optomechanical interaction between light and molecular vibrations. We demonstrate an experimental platform composed of a plasmonic nanocube-on-mirror antenna coupled to an open, tunable Fabry-Perot microcavity for selective addressing of individual vibrational lines of molecules with strong Raman scattering enhancement. Multiple narrow and intense optical resonances arising from the hybridization of the cavity modes and the plasmonic broad resonance are used to simultaneously enhance the laser pump and the local density of optical states, and are characterized using rigorous modal analysis. The versatile bottom-up fabrication approach permits quantitative comparison with the bare nanocube-on-mirror system, both theoretically and experimentally. This shows that the hybrid system allows for similar SERS enhancement ratios with narrow optical modes, paving the way for dynamical backaction effects in molecular optomechanics.

INTRODUCTION

Surface-enhanced Raman spectroscopy (SERS) (*1*–*3*) is a powerful spectroscopy method that relies on the extreme field confinement of metallic plasmonic surfaces to strongly enhance Raman scattering by a molecule (*4*, *5*). Recently, SERS has been described within the framework of cavity optomechanics (*6*–*8*). This viewpoint gives a picture of the optical forces of the plasmon resonator mode onto the molecule's mechanical modes, providing an explanation for various proposed and observed effects such as parametric cooling or amplification of the mechanical motion, and hence nonlinear SERS enhancements (*9*–*11*), as well as coherent infrared-visible conversion (*12*, *13*). Most of the promises contained in this vista of cavity optomechanics transposed to molecular vibrations require the sideband-resolved regime, where the optical resonance linewidth is narrow compared to the mechanical vibrational frequency of the molecules. This allows controlling the phase of the optomechanical interaction, selectively enhancing or suppressing Stokes or anti-Stokes scattering processes through dynamical backaction of the optical resonance (*14*). Because of the large decay rate of plasmonic resonances, the electromagnetic enhancement offered in SERS is intrinsically broad, limiting the coherence of the optomechanical interaction. While the low-quality factors (Q) of plasmonics mean that sideband-resolved plasmonic SERS is out of reach, recent work has argued that sideband-resolved SERS is possible via the use of a hybrid plasmonic-photonic resonator, both theoretically (*15*, *16*) and experimentally (*17*). A hybrid resonator combines a high-Q photonic resonator with a low mode volume plasmonic resonance (*18*–*21*). The resulting resonances are narrower than the usual molecular vibrational resonance frequencies, allowing for sideband-resolved SERS with single optical resonators and strong SERS enhancements (*16*, *22*).

The single realization to date (*17*), however, relied on lithography to define both the resonator and the plasmonic antenna. Lithographic methods suffer two major drawbacks: They face a roadblock in terms of SERS enhancement due to inherent poor field confinement obtained with antenna gaps in the range of tens of nanometers, and they are limited to a single cavity mode for hybridization, precluding simultaneous pump and Raman emission enhancement, mandatory to reach potential breakthrough molecular optomechanics applications. New architectures that leverage the best plasmonic SERS structures such as ultra-narrow gaps and atomically controlled metallic facets are needed (*23*, *24*), with tunable multimode operation that could aim toward single-molecule sideband-resolved SERS.

Here, we report selective Raman enhancement in a new generation of hybrid resonators that combine state-of-the-art gap antenna modes (*25*) together with a tunable Fabry-Pérot (FP) cavity (*26*). This system allows reaching record SERS enhancements beyond 10^{10} in a sideband-resolved regime, with the possibility to tune the hybrid mode resonance frequency in situ and, thus, independently and selectively enhance single Raman lines. The gap antenna is made directly on one of the two FP mirrors and is essentially the well-known nanocube-on-mirror (NCoM) geometry with all its electromagnetic and structural advantages (*25*, *27*). The bottom-up fabrication approach that we adopt allows for a full comparison of the hybrid cavity performance with the bare constituents from which it is made and, in particular, with the bare NCoM system. We show that the tunable hybrid SERS performance is at least equivalent in strength to the one of the ideal nanoantenna system, with room for an improvement of three orders of magnitude in SERS enhancement factor up to 10^{13} by optimizing the reflectors and reducing the height of the spacer that forms the gap. This opens

[1]Department of Information in Matter and Center for Nanophotonics, AMOLF, Science Park 104, 1098 XG Amsterdam, Netherlands. [2]Matériaux et Phénomènes Quantiques, Université Paris Cité, CNRS UMR 7162, Paris, France. [3]Single Quantum B. V., Rotterdamseweg 394, 2629 HH Delft, Netherlands. [4]Institute of Physics, University of Amsterdam, 1098 XH Amsterdam, Netherlands.
*Corresponding author. Email: f.koenderink@amolf.nl

up the perspective of sideband-resolved single-molecule SERS and of high optomechanical cooperativities with molecules.

RESULTS

We realize the system as depicted in Fig. 1 as a tunable hybrid cavity, displaying both a strong field confinement and a high-quality factor. The system consists of a monocrystalline gold nanocube on top of a flat gold mirror forming an NCoM system (*27*), embedded in a tunable, open-access FP microcavity interferometer (*28*, *29*), and will be designated as NCoM-in-FP. The NCoM system exhibits an in-plane magnetic dipole mode that radiates vertically away from the mirror (*30*, *31*). This mode has a broad resonance and exhibits very high local density of states (LDOS) in the middle of the gap. The gold cube is separated from the mirror by a thin Al_2O_3 dielectric spacer layer whose thickness can be tuned (1 to 15 nm) to control the gap resonance frequency. By placing the NCoM in an FP cavity, created by a second concave mirror, the cavity mode and plasmon antenna mode hybridize, combining the electromagnetic field spatial confinement and LDOS of the NCoM system and the narrow resonance of the FP cavity. This hybrid mode realizes mode volumes V_m of around $10^{-4}\ \lambda^3$ and Q factors of ≈300. The hybrid resonator is used to selectively address individual vibrational modes of molecules. More specifically, monolayers of biphenyl-4-thiol (BPT) are self-assembled on the cube, automatically placing these molecules in the region where the strong field enhancement from the NCoM is present. By virtue of the small linewidth of the hybrid optical mode, it becomes possible to achieve sideband-resolved SERS and have well-controlled optomechanical interaction. The optical resonances can be tuned with the cavity opening so that it can enhance both the pump laser and a single vibrational line. To this end, the free spectral range (FSR) is matched to the vibrational energy of the molecule such that one cavity mode matches the pump wavelength, and another matches the vibrational line of interest.

To elucidate the design characteristics, we discuss COMSOL simulations of first the NCoM system, then the FP microcavity, and finally the hybrid system. We performed modal analysis to understand the hybridization of the NCoM system with the cavity mode. To this end, we use the so-called quasi-normal mode (QNM) formalism in the implementation reported by Yan *et al.* (*32*).

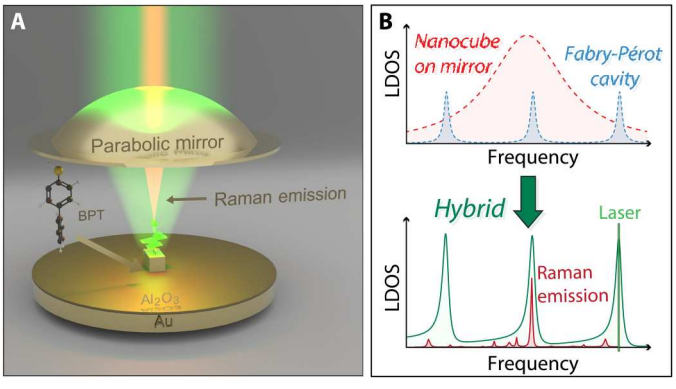

Fig. 1. The nanocube in an FP hybrid resonator. (**A**) We realize a bottom-up hybrid resonator for SERS that leverages the self-assembled NCoM system for confinement, embedding it in a tunable FP cavity for tunability and sideband resolution. The nanocube is coated with BPT molecules, whose Raman emission enhancement can be tuned by changing the cavity mirror spacing. (**B**) Schematic representation of the tunable dual SERS enhancement obtained with the hybrid resonator, offering both pump and LDOS enhancement with sideband resolution.

The NCoM system supports several modes that have strong field confinement in the gap (*30*). Our mode of interest is an (11) mode with an in-plane magnetic dipole mode in the center of the gap, visible in Fig. 2A. The resonance frequency of this mode can be tuned by varying the spacer layer thickness or the cube dimensions. For an Al_2O_3 spacer thickness of 6 nm, a cube side length of 75 nm, and a semitransparent 30-nm gold mirror, the LDOS and radiation pattern of the (11) mode are shown in Fig. 2 (B and C) and display a resonance wavelength near 820 nm. The LDOS is calculated near the edge of the cube, 1 nm below the cube, where the molecules are expected to be located. LDOS enhancement values of up to 24,000 are reached at $Q = 22$, which correspond to mode volumes of order $1.3 \times 10^{-5}\ \lambda^3$. The LDOS has a relatively high radiative contribution of around 34% despite the nanometer gaps and despite the unconventional choice of just a thin 30-nm Au mirror (*33*). This thin mirror is chosen such that in experiments we have transmission through the mirror, which enables imaging the location of the nanocubes inside the cavity by looking from outside the cavity through the mirror (*34*). The radiation pattern of the (11) mode has a strong lobe perpendicular to the mirror, as shown in Fig. 2B, with an angular full width at half maximum (FWHM) of 45°. This radiation pattern is well matched to the modest numerical aperture (NA) parabolic mirror that we will use to close the microcavity, and is hence advantageous for efficient hybridization with cavity modes. For reference, the radiation pattern of the vertical dipole mode (10) is also shown. It has a radiation pattern whose maximum is at 60° away from the surface normal, quite unsuited for hybridization with an FP mode.

Next, we report on the microcavity properties that one can obtain with a 30-nm-thick flat gold mirror and a 30-nm-thick parabolic mirror, also from gold and with a radius of curvature of 8 μm. Electric and magnetic field intensities for a typical cavity mode are shown, as well as cavity transmission, in Fig. 2 (D and E). We focus on the fundamental transverse modes at low longitudinal mode numbers m. The cavity resonances in the near infrared for a 3-μm cavity opening (yielding an FSR of 110 nm) feature optical quality factors of ca. 250 mainly limited by the mirror thickness. The magnetic field experiences a maximum at the mirror surface, naturally matching the in-plane magnetic dipole of the (11) mode of the cube, making it ideal for hybridization.

The electric and magnetic field profiles of the hybrid resonator mode combining the NCoM in an FP cavity are shown in Fig. 2F, where we recognize the $m = 2$ cavity mode, obtained for an 800-nm opening of the cavity. The hybrid character of the selected mode is demonstrated by the strong field components in the nanogap that are typical of NCoM systems. The LDOS, mode volume, and Q of the hybrid mode depend on the spectral detuning between the NCoM and the cavity resonances. Taking hybrid mode volumes from the quasi-normal mode formalism (*35*), we find values on the order of $V_m \sim 10^{-4}\ \lambda^3$ and $Q \sim 100$. The hybrid resonator will thus allow reaching sufficiently narrow linewidths to enhance single vibrational modes of the molecule, with only a modest loss in field confinement compared to the NCoM without the closing

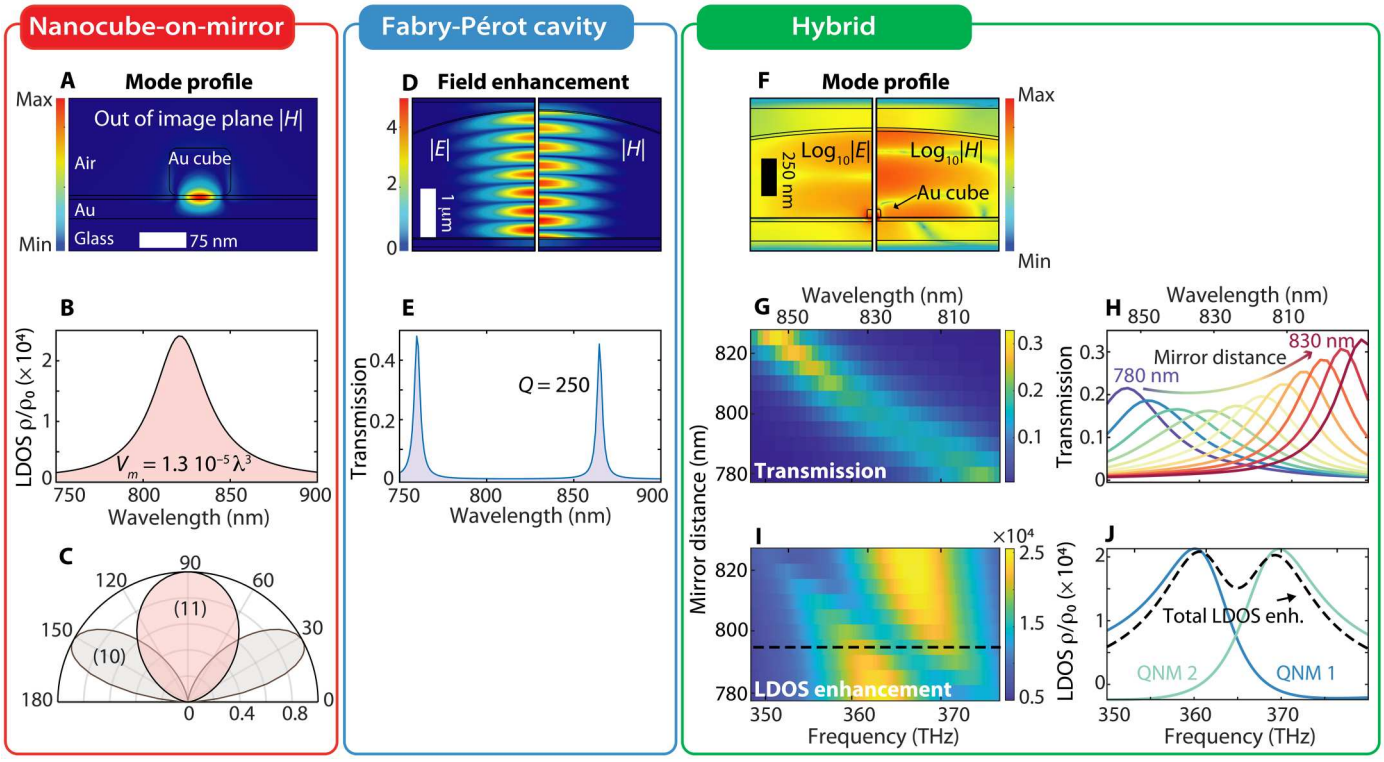

Fig. 2. Simulation results obtained with COMSOL and quasi-normal modal analysis, comparing the NCoM antenna, the empty FP cavity, and the hybrid resonator metrics. Analysis performed with the MAN package (*32*). (**A**) Magnetic mode (11) profile of the NCoM tuned into resonance by a 6-nm alumina gap, featuring (**B**) a strong LDOS enhancement with respect to a homogeneous alumina environment (ρ/ρ_0) for a vertical dipole placed below the corner and in the middle of the gap. (**C**) Normalized radiation pattern of the magnetic (11) mode (red) with a vertical radiation direction as opposed to the usual dipolar (10) mode radiation pattern (light brown) with a mostly tangential radiation. (**D**) Field enhancement in the empty FP cavity obtained by placing a curved mirror on top of a flat gold mirror [30-nm thickness as in (A) to (C)], illuminated by a 1-μm-waist Gaussian beam. (**E**) Transmission spectrum of the bare cavity showcasing *Q* factors greater than 200 for 30-nm-thick gold mirrors. (**F**) Mode profiles of the NCoM in an FP cavity hybrid. The individual constituents are coupled through their strong *H* fields on the mirror surface. (**G** and **H**) Transmission spectra of the hybridized cavity structure for varying mirror distances. The linewidth and resonance frequency change as a function of the detuning with the NCoM. (**I**) Total LDOS enhancement for a vertical dipole placed in the middle of the gap below the cube's corner reaching values up to those obtained with the bare NCoM, but with an additional control on the quality factor and resonance frequency. (**J**) Crosscut of (I) for the FP cavity and the NCoM at resonance: The total LDOS (dashed) is a sum of contributions of two hybridized quasi-normal modes, whose asymmetric shape arises from complex valued mode volumes (*38*).

mirror (one order of magnitude higher mode volume, very similar LDOS values).

The properties of the hybrid resonances are explored by mapping the LDOS at 1 nm below the cube corner as a function of frequency and for different cavity openings (Fig. 2I). The LDOS reaches high values above 10,000, of the same order as the values calculated for the bare NCoM and an order of magnitude higher than the state-of-the-art demonstrated hybrid plasmonic-photonic resonators (*17*). For high-*Q* microcavities coupled weakly to dipolar nanoantennas, it has been reported that the LDOS follows Fano line shapes (*16*, *20*, *36*), evident as very sharp and asymmetric features on the broad background of the plasmon resonances. The diagram obtained for the LDOS in this system may visually suggest an anti-crossing between two resonances but should not be interpreted as strong coupling. Instead, Fano features appear in the same spirit as in previous work (*18*, *37*), with the main difference that the contrast between quality factors is smaller in our system since the cavity *Q* is only one order of magnitude larger than that of the antenna. This results in comparatively smooth LDOS variations near the cavity frequency. Figure 2J shows the LDOS spectrum when the cavity is on resonance with the antenna mode. The system exhibits two maxima in LDOS, which, using QNM theory, we can decompose as being due to two hybridized eigenmodes. From a fit of the LDOS two-dimensional map and using a semianalytical model (*16*), we conclude that there is a hybrid coupling constant $J/2\pi = 3.5$ THz (see the Supplementary Materials) to be compared with damping rates $\kappa/2\pi = 5$ THz and $\gamma/2\pi = 17$ THz for the cavity-like and antenna-like modes. These values indicate that the system is not considered to be in the strong coupling regime since the optical coupling strength between the two subsystems is still smaller than both of the linewidths. The interaction between the two modes results in non-Lorentzian line shapes for the LDOS, typical of interference effects in dissipative, multimode systems (*38*), which can also display negative contributions of a single mode to the total LDOS. This can be quantified by the complex nature of the mode volume derived from QNM analysis (*35*), which here reaches notable non-real values up to $\mathrm{Im}(V_m)/\mathrm{Re}(V_m) \simeq 1$. In this system, they arise mainly because of the interaction of the two modes since for each bare constituent separately (the FP cavity or even the NCoM antenna), the mode volume is mostly real [$\mathrm{Im}(V_m)/\mathrm{Re}(V_m) < 0.1$]. This demonstrates the possibility of using hybrid resonators to investigate dissipative coupling in molecular

optomechanics, where the optical cavity resonance modulates the damping rate of a molecular vibration, which can significantly facilitate reaching high cooperativity regimes (*39*).

The simulated transmission of an incident Gaussian beam through the hybrid system is shown in Fig. 2 (G and H). When tuning the cavity frequency over the NCoM resonance frequency, the main effect is a modest decrease in quality factor. While this observation is in remarkable contrast to the strong feature in the LDOS map, the predicted small variation in transmission is commensurate with cavity perturbation theory (*28*, *40*, *41*). Cavity perturbation theory predicts a complex-valued cavity frequency shift that is proportional to the antenna polarizability, and is hence expected to be fully imaginary for on-resonance coupling. The resulting reduction in Q is mainly visible as a variation in the maximum cavity transmission—the choice of 30-nm-thick mirrors allows reaching good maximum theoretical transmission of around 30% and is ideal for our SERS experiments, but the intrinsically modest cavity Q is clearly not optimal for studies mapping cavity perturbation theory.

Next, we turn to experimental realization of the proposed platform. First, we fabricate flat mirrors by physical vapor deposition of 30 nm of Au on glass, over which we apply a thin spacer of Al_2O_3 using atomic layer deposition (15 monolayers). This spacer is precisely chosen to place the NCoM resonance frequency [see (*42*) for experimental tuning calibration] between the pump and the Stokes sideband so as to increase the white-light (WL) signature of hybridization, and at the same time allowing for a fair comparison of the hybrid with respect to the bare NCoM construct. To facilitate cavity alignment, the flat mirrors in our experiment are mesas carved out of a glass substrate. The NCoM system is formed by dropcasting 70-nm gold nanocubes (Fig. 3B), which have been previously functionalized with BPT molecules by self-assembly over a 12-hour incubation period. For the second mirror forming the FP cavity, we use concave mirrors, fabricated by CO_2 laser ablation of glass (*26*, *43*) and subsequent coating by physical vapor deposition of 30 nm of gold. From atomic force microscopy (AFM) measurements of the fabricated concave features, we estimate an NA = 0.24, a radius of curvature of R = 9 μm, and a roughness before coating of below 0.5 nm.

To interrogate the system, we use a microscope setup that can perform measurements in transmission and reflection (Fig. 3A). At the heart of the setup is an assembly of micromechanical stages for positioning the curved mirror and the flat mirror relative to each other, and in the focus of the microscope objectives (XYZ and tip/tilt degrees of freedom). For the flat reflector, XYZ piezo actuation assures fine positioning of the cube, also allowing us to compare NCoM systems and flat mirror responses without modifying the setup. The curved reflector can be scanned such that we tune the cavity opening. Mechanical drifts of around 10 pm/s result in cavity frequency instabilities of $20/m$ pm/s, with m the cavity mode order. The setup is equipped with a supercontinuum white light source and with a narrowband tunable diode laser (Toptica DL-Pro 780, 50-nm tuning range) as Raman pump laser. A galvanic mirror system allows for confocal imaging and fine positioning of the excitation spot. We use a camera for positioning and alignment, and a fiber-coupled Andor spectroscopy system (Andor Shamrock A-SR-303i-B-SIL) equipped with a cooled silicon charge-coupled device (CCD) camera (Andor iVac A-DR324B-FI) for spectroscopy. The Raman pump light is rejected with a set of two notch filters (Thorlabs NF785-33). This setup allows for dark-field scattering, cavity transmission, and SERS measurements—all in both reflection and transmission. Moreover, in the same setup, we can compare cavity-NCoM performance with the bare NCoM system performance measured on the same nanocube. Last, markers in the sample allow comparing individual cube data to scanning electron micrographs, and to extinction spectra that we take in a separate setup reported in (*42*).

First, we plot the extinction spectrum of a bare NCoM in Fig. 3C, obtained using a low NA objective. It shows the response to the supercontinuum laser, filtered with an acousto-optical tunable filter (Crystal Technologies) over approximately 5 nm, whose center frequency is scanned. We obtain a resonance with Q = 17 similar to what is expected from the simulated LDOS for the (11) NCoM mode. For the same cube, Fig. 3D shows a bare NCoM SERS spectrum. The SERS spectrum (with the region around the pump wavelength blocked by a notch filter) shows a broad and featureless line shape that is very close to the cube extinction resonance, and which we interpret as the SERS-enhanced electronic Raman signature of gold (*44*). Vibrational Raman lines of BPT appear on top of this background. The anti-Stokes signature is, in this case, less significant because of the red detuning of the cube resonance relative to the pump wavelength. Figure 3 (E to G) highlights properties of the cavity system in the absence of any cube. In Fig. 3F, we report transmission versus wavelength as we open and close the microcavity using a saw-tooth voltage applied to the z-piezo. A tapestry of cavity transmission resonances is clearly evident, with the main bright lines corresponding to fundamental modes of different longitudinal mode number. The fainter features in between the bright resonances are due to higher-order transverse modes. This interpretation is confirmed by real-space imaging of the cavity output in transmission on a camera. Figure 3G reports transmission at a fixed cavity opening of 1.5 μm, showing that we can routinely access longitudinal mode orders down to m = 3 and above (up to m = 10 typically), with Q factors scaling from 100 to 300.

We can now assemble hybrid resonators and perform mode scatterometry and SERS. Figure 4A shows transmission versus wavelength of a cavity of fixed geometry with and without a metal nanoantenna. We accomplish this by sideways movement of the flat mirror to scan the nanoantenna into and out of focus of the cavity. We observe a small red shift of the cavity resonances, and evidence for a reduction in cavity Q, through a broadening and a reduction of the transmission peak height. As per Fig. 2, we expect mainly a Q-factor reduction in the present operating regime. The Q drops approximately from 280 to 220, as expected for an m = 5 mode and a hybrid coupling strength of $J/2\pi$ = 2 THz. The presence of the nanoparticle also results in a dispersive shift of the cavity frequency due to a modification of the optical path length. This is best visualized when plotting the shift of the FSR Δf_{FSR} normalized by the resonance frequency f_m as shown in Fig. 4B. $\Delta f_{FSR}/f_m = 1/m$ is a constant that does not depend on the cavity opening and allows to get rid of the instabilities arising from the lateral piezo movement. Since for each cavity mode the frequency shift depends on the detuning with the nanoparticle, the normalized FSR is shifted when the cube is scanned laterally through the cavity. Both the linewidth increase and the dispersive shift are observed over a lateral displacement distance of around 1 μm. This distance is given by the lateral extent of the cavity mode at the mirror.

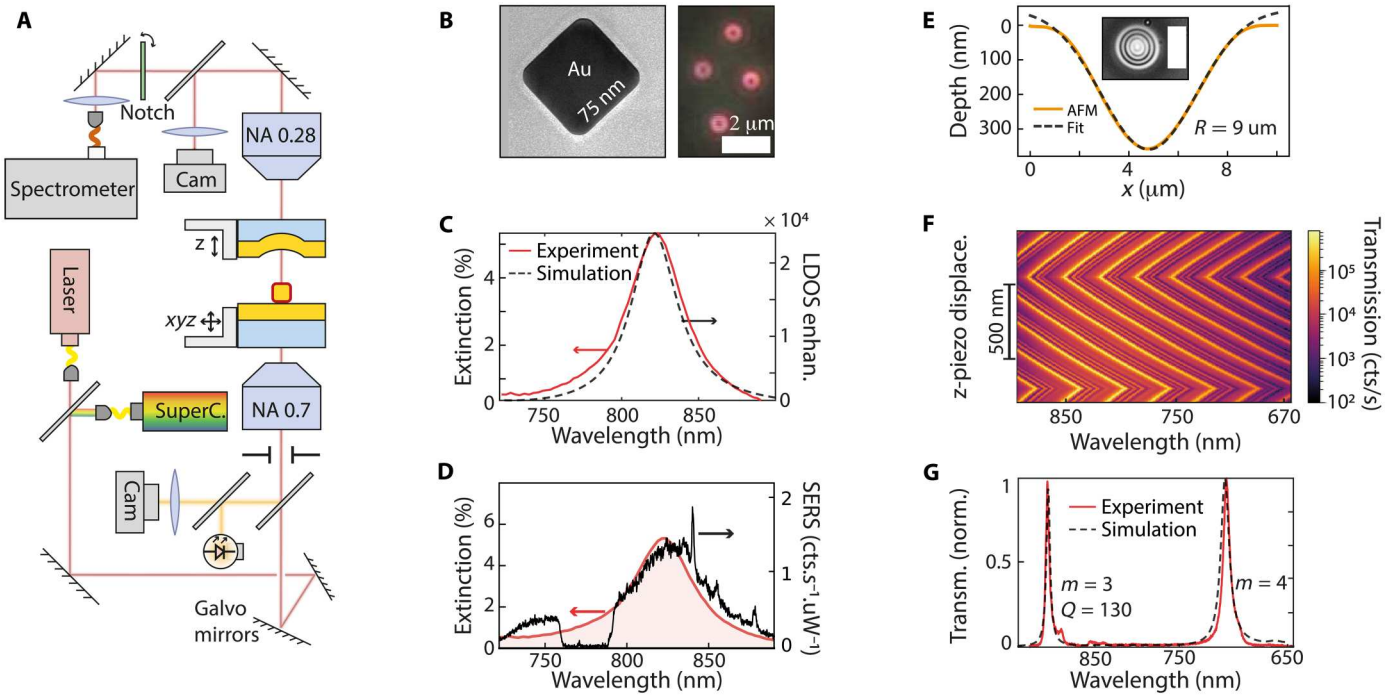

Fig. 3. Optical characterization of the bare constituents. (**A**) Homebuilt confocal Raman and white-light spectroscopy setup working in both reflection and transmission. The sample position is controlled with two sets of piezos allowing cavity and NCoM alignment. The SERS excitation laser is tunable to match the cavity, while the cavity opening tunes the cavity resonance and FSR. (**B**) Transmission electron microscopy image of a typical nanocube and dark-field image of NCoM structures. (**C**) Extinction spectrum of a bare NCoM whose resonance frequency is tuned to 820 nm using a 2-nm alumina gap. The LDOS enhancement spectrum simulated for a dipole under the cube corner is shown for comparison (dashed). (**D**) SERS spectrum (black line) taken on the same NCoM displays a broad background from electronic Raman of the gold with a spectral shape similar to the extinction spectrum (red). The distinct peaks above it are characteristic Raman lines of BPT molecules that were previously coated on the nanocube. (**E**) Atomic force micrograph of the curved mirror fabricated using CO_2 laser ablation, which results in curved and smooth ~300-nm-deep concave features with a radius of curvature of about 9 μm. The inset shows a camera image of the bare cavity in transmission (scale bar, 10 μm). (**F**) Measured transmission spectra of a bare cavity for a saw-tooth displacement of the z-piezo that controls the cavity opening, which allows tuning the cavity modes resonance. (**G**) Transmission spectrum for a fixed mirror distance of 1.5 μm. A cavity resonance with Q = 130 at the m = 3 longitudinal mode order is extracted from a Lorentzian fit.

Figure 4D shows Raman spectra of the sample where the pump laser wavelength is fixed at 771 nm, and we modulate the cavity length back and forth. In general, the vibrational lines of BPT, which should appear as vertical features in the diagram (since the laser is fixed), are hardly visible because of the fact that when used off-resonance, the cavity transmission function blocks the pump and the signal, making efficient pumping and signal collection impossible. Nonetheless, the fact that we scan the cavity is evident as faint diagonal stripes, indicative of enhancement of the electronic and molecular SERS by the fundamental and higher-order cavity resonances. Whenever a hybrid cavity resonance overlaps with a molecular line (e.g., at 841 nm for the blue circle), a bright burst of SERS signal is collected, indicating hybrid enhancement of the SERS signal. Single crosscuts for SERS enhancement of three different individual vibrational lines are shown in Fig. 4E and correspond to the spectra at the position of the bright spots marked by circles in Fig. 4D. They correspond to the 1079, 1281, and 1586 cm^{-1} BPT Raman lines, respectively, and illustrate how the cavity allows for selective enhancement of the Raman signal by modifying the LDOS frequency landscape felt by the molecules.

Next, our ambition is to optimize the use of the selective cavity-enhanced plasmonic SERS and to quantify the performance relative to standard NCoM SERS. First, we realize that in Fig. 4, the performance is limited because the system offers a cavity resonance at the Raman-shifted frequency but does not also offer a hybrid resonance for pump enhancement. Second, to quantify performance, we perform quantitative count rate comparisons for cubes with and without the closing cavity mirror. Figure 5 summarizes the results, with a direct correlative comparison white-light response of the resonator and the resulting SERS spectra.

The results for the reference NCoM [cube geometry verified by scanning electron microscopy (SEM)] without the top mirror are shown in the first column. Figure 5A shows the extinction spectrum featuring the broad Lorentzian resonance of the NCoM (11) mode. The SERS response shown in the bottom panel, taken with the NA = 0.7 objective from the air side of the NCoM, follows closely this resonance and features enhancement of both gold electronic Raman and the BPT lines.

Figure 5 (C and D) shows, respectively, cavity transmission and Raman spectra measured in transmission for the hybrid structure. For each column of graphs, one cavity mode is tuned to enhance the pump, while at the same time the FSR is tuned so that a second mode enhances the 1079, 1281, and 1586 cm^{-1} lines, successively. Not only is sideband resolution obtained, with sideband resolution $\Omega_m/\kappa_{eff} = 25$ (where κ_{eff} is the cavity linewidth broadened by hybridization), but the relatively good Q of the cavity allows for specific vibrational line enhancement at will. All measurements are obtained for the same sample by simply varying the cavity opening.

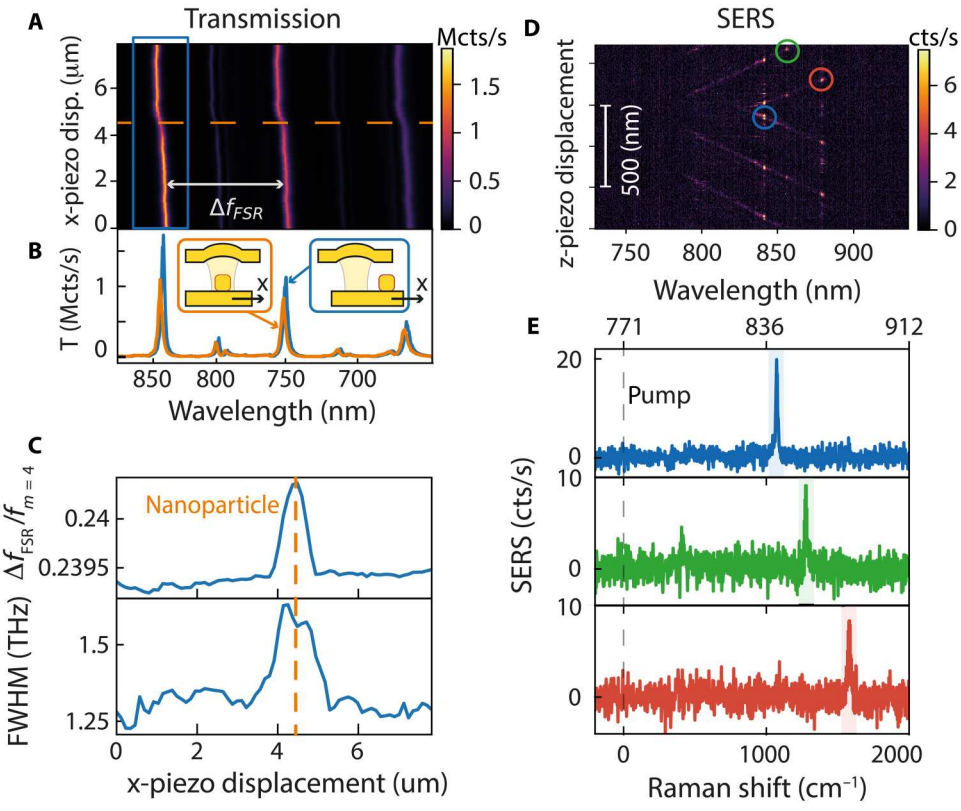

Fig. 4. Signature of hybridization and selective LDOS enhancement. (**A**) Cavity transmission spectra when laterally displacing a nanoparticle from the outside into the cavity space. (**B**) Crosscuts comparing the bare cavity transmission (blue) with the hybridized cavity transmission [orange curve, corresponding to the dashed line in (A)]. (**C**) Variations in FSR and linewidth of the $m = 4$ cavity resonance [blue box in (A)] as a function of cube position, showing how the nanoparticle induces a dispersive and dissipative shift of the cavity resonance. (**D**) Raman spectra of the same hybrid for varying mirror distances. This allows selectively enhancing single Raman peaks of the BPT molecules. (**E**) Crosscuts corresponding to the selective enhancement of three main BPT Raman peaks indicated by circles in (D).

The Raman signal also shows enhancement of electronic Raman background from higher transverse order cavity modes that are only weakly visible in cavity transmission. They arise from slight imperfections of the cavity (slightly tilted mirrors, non-Gaussian curvature) and from the NCoM not being exactly positioned at the exact center of the cavity.

For both the hybrid resonator and the bare NCoM system, the same input laser power of 200 μW has been used; it is remarkable that, essentially, the same SERS count rates at given input power are obtained for the NCoM and the hybrid resonator, despite the fact that pumping and collection are now through two partially opaque metallic films and at a much lower NA (collection NA for the cavity transmission is 0.28). This eliminates the hypothesis of a cavity simply acting as a transmission filter for the Raman signal produced by the NCoM, since in that case, one would obtain at least a 20 times reduction in signal (5% of cavity transmission measured at resonance) with an additional reduction related to mismatch between collection NA and NCoM emission pattern. Consistent with the observed similar count rates, a detailed analysis presented in the Supplementary Materials shows that the hybrid resonator allows reaching SERS enhancements that are equivalent to SERS enhancements obtained with bare NCoMs in optimal experimental settings but with the important feature of working well beyond the sideband-resolved regime. The estimated SERS enhancement factor for both structures when considering input and output coupling efficiencies is above 10^7.

DISCUSSION

We presented a novel tunable hybrid resonator consisting of an NCoM plasmonic antenna placed inside an FP cavity and benefiting from both the strong electromagnetic enhancement in the gap and the high-Q tunable resonance of the cavity. The resonance frequency of the hybrid mode can be tuned by changing the cavity opening, allowing enhancing specific Raman lines and placing the system well inside the sideband-resolved regime. The hybridization has been first rationalized using a rigorous modal analysis and finite element modeling, which also showed the potential of this structure to study dissipative optomechanical coupling (*39*). Experimental demonstration of in situ tunable sideband-resolved SERS using gap plasmonic modes has been shown. A quantitative comparison of the hybrid resonator and the bare nanoantenna resonator performance allowed by our bottom-up fabrication approach shows that the SERS enhancements of the hybrid outperforms the NCoM, owing to its two cavity modes resonantly enhancing both pump and Raman emission, as underpinned by the semianalytical model presented in the Supplementary Materials.

Further optimization by several orders of magnitude is possible by considering the tuning of the NCoM resonance wavelength. We

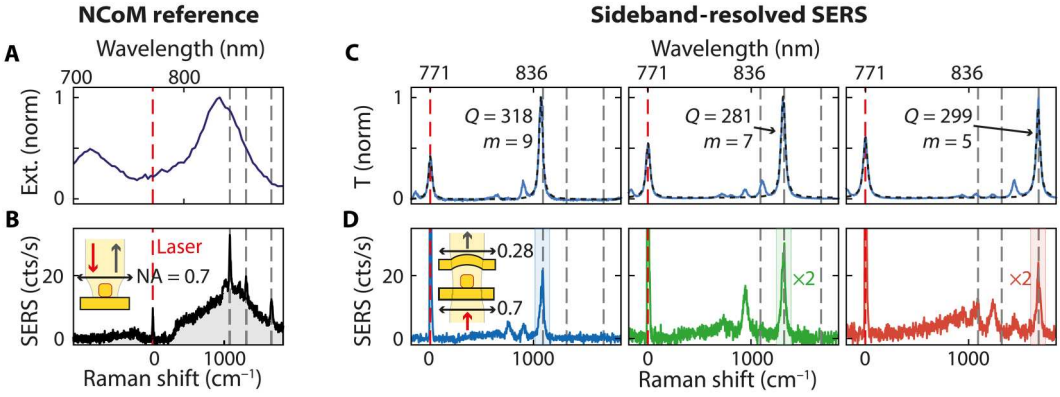

Fig. 5. Comparing NCoM and hybrid performances. (**A**) NCoM extinction spectrum and (**B**) corresponding SERS signal. (**C**) Hybrid resonator transmission spectra with three distinct cavity opening lengths. (**D**) Corresponding SERS spectra with a distinct Raman line enhanced in the three different panels. Both the pump field and the LDOS for Raman emission are enhanced in each of the cases, as we match the cavity FSR to the Raman shift by adjusting the cavity opening. The pump light matches a first resonance, while strong Raman scattering is only obtained for molecular vibrational lines that are specifically tuned to the second cavity resonance.

have chosen to work with NCoMs with resonances tuned between the laser pump and the Raman line wavelengths, not because it is optimal for the hybrid resonator, but because it is optimal for the bare nanoantenna system and also because it results in the strongest white-light transmission signatures of hybridization as shown in Fig. 4. Thus, this choice allows for a conservative comparison between the hybrid resonator and the nanoantenna. Nonetheless, even for large cavity-antenna detunings (on the order of a few antenna linewidths), the hybridized cavity mode can sustain high LDOS and field enhancement values on par with the maximum values obtained for the bare NCoM (*20*). This unique property can be used to maintain sideband resolution with the cavity mode while reducing undesired photon scattering into the broad antenna mode by working with a far detuned antenna with respect to the pump and the Raman lines. This can, for example, allow us to strongly enhance the Stokes process while avoiding most of the anti-Stokes scattering, leading to phonon buildup and nonlinear Raman scattering (*6*). For example, by red-detuning the antenna by two antenna linewidths ($\omega_L - \omega_a = 2\gamma$), the total anti-Stokes scattering can be suppressed by a factor of 40 compared to the resonant antenna case while reaching a similar Stokes scattering rate than the resonant antenna (see the Supplementary Materials). Inversely, in the opposite configuration, the hybrid can be used to strongly suppress the Stokes process, which is required to reduce the laser-related noise in mid-infrared (IR) upconversion schemes (*12*, *13*, *45*).

Overall, the optomechanical cooperativity of the hybrid resonator is just limited by the performance of the antenna mode that is used, and by reducing the gap size of the NCoM system down to the single-digit nanometer scale (which would advantageously red-detune the antenna mode at the same time), one could tend toward SERS enhancement factors of order 10^{13} paving the way for integrated sideband-resolved single-molecule SERS (*46*, *47*), and for the high optomechanical cooperativity regime necessary for low-noise upconversion or to observe nonlinear effects (*9*, *11*) such as phonon lasing. The NCoM-in-FP multimode geometry is also a perfect candidate for multitone optical driving, which provides prospects of studying squeezed mechanical states or demonstrating entanglement of multiple molecular mechanical resonances (*48*, *49*). Collective effects and even stronger coupling are within reach by inserting multiple cubes coupled through the same cavity mode.

MATERIALS AND METHODS

Fabrication

For the NCoM, a quartz substrate is pretreated, where a platform elevated from the rest of the substrate by a few hundred micrometers is created using a water jet and facilitates the cavity alignment. After that, electron-beam evaporation is performed using a Polyteknik E-Flex, depositing 30-nm Au at a deposition rate of 0.5 Å/s. A 2-nm adhesion layer of Cr is used. The thickness of the gold layer is a compromise between visibility of the cubes in microscopy and the quality of the plasmonic cavity. An Al_2O_3 spacer layer of variable thickness is grown on top. We dropcast nanocubes (75 nm nominal, Nanopartz), previously incubated for 12 hours in a 1 mM BPT solution in anhydrous ethanol to form a self-assembled molecular monolayer, and performed dark-field microscopy to verify successful assembly of the NCoM system. The typical single-cube radiation pattern in dark-field microscopy, observed for a spacer of 2 nm, is shown in Fig. 3C. The donuts are observed for a high-NA dark-field objective, where the WL impinges the sample only at high angles. For lower NA, we collect the magnetic mode 11, which gives filled round shapes. Each structure is imaged on the SEM to verify that the nanoparticle under study corresponds to a single nanocube. This step is done after all the SERS measurements have been performed to avoid molecule damage from the electron beam.

For the curved mirror, we use CO_2 laser (Synrad 48-1 working at λ = 10.6 μm) ablation to create concave mirrors. We use a home-built setup in which we focus a pulse of 100 ms and 300 mW to a tight spot using an IR lens (black diamond, NA = 0.5, Thorlabs). We tune the exposure dose and focusing to obtain mirrors with a radius of curvature of around 9 μm and a depth of 350 nm. These mirrors can subtend an NA of 0.25. We verified the mirror topography by AFM (Veeco Dimension 3100), observing a roughness below 0.5 nm.

Optical setup

The measurements are performed on a homebuilt confocal Raman spectroscopy setup shown in Fig. 3. White-light extinction and transmission spectra are obtained using a supercontinuum laser (Fianium WL-SC-390-3) and detected with a fiber-coupled spectrometer (Andor Shamrock A-SR-303i-B-SIL) equipped with a cooled silicon CCD camera (Andor iVac A-DR324BFI). The laser is focused using a Nikon, glass-compensated, 60× objective (NA = 0.7) and collected by the same objective when working in reflection or by a long working distance Mitutoyo 10× Plan APO objective (NA = 0.28) when working in transmission. Excitation for the Raman spectra is performed with a narrowband tunable diode laser (Toptica DL-Pro 780), spectrally cleaned with a pair of band-pass filters (Semrock TBp01-790/12). Before insertion of detected light into the collection fiber, Rayleigh scattered light is filtered with a set of two notch filters (Thorlabs NF785-33). Laser power is set to 200 μW, and the spectra are integrated over 1 s. The cavity is aligned with a set of three-stage piezoelectric translations (Jena Tritor) for the planar mirror containing the nanocubes, and a linear *z*-piezoelectric stage (Nanofaktur PPO) for the curved mirror.

Supplementary Materials

This PDF file includes:

Supplementary Text
Figs. S1 to S4
Tables S1 and S2
References

REFERENCES AND NOTES

1. D. L. Jeanmaire, R. P. Van Duyne, Surface raman spectroelectrochemistry: Part I. Heterocyclic, aromatic, and aliphatic amines adsorbed on the anodized silver electrode. *Electrochemistry* **84**, 1–20 (1977).
2. A. Otto, I. Mrozek, H. Grabhorn, W. Akemann, Surface-enhanced Raman scattering. *J. Phys. Condens. Matter* **4**, 1143–1212 (1992).
3. R. Pilot, R. Signorini, C. Durante, L. Orian, M. Bhamidipati, L. Fabris, A review on surface-enhanced Raman scattering. *Biosensors* **9**, 57 (2019).
4. M. Moskovits, Surface-enhanced Raman spectroscopy: A brief retrospective. *J. Raman Spectros.* **36**, 485–496 (2005).
5. K. A. Willets, R. P. Van Duyne, Localized surface plasmon resonance spectroscopy and sensing. *Annu. Rev. Phys. Chem.* **58**, 267–297 (2007).
6. P. Roelli, C. Galland, N. Piro, T. J. Kippenberg, Molecular cavity optomechanics as a theory of plasmon-enhanced Raman scattering. *Nat. Nanotechnol.* **11**, 164–169 (2016).
7. R. Esteban, J. J. Baumberg, J. Aizpurua, Molecular optomechanics approach to surface-enhanced Raman scattering. *Acc. Chem. Res.* **55**, 1889–1899 (2022).
8. M. K. Schmidt, R. Esteban, F. Benz, J. J. Baumberg, J. Aizpurua, Linking classical and molecular optomechanics descriptions of SERS. *Faraday Discuss.* **205**, 31–65 (2017).
9. F. Benz, M. K. Schmidt, A. Dreismann, R. Chikkaraddy, Y. Zhang, A. Demetriadou, C. Carnegie, H. Ohadi, B. De Nijs, R. Esteban, J. Aizpurua, J. J. Baumberg, Single-molecule optomechanics in "picocavities". *Science* **354**, 726–729 (2016).
10. A. Lombardi, M. K. Schmidt, L. Weller, W. M. Deacon, F. Benz, B. de Nijs, J. Aizpurua, J. J. Baumberg, Pulsed molecular optomechanics in plasmonic nanocavities: From nonlinear vibrational instabilities to bond-breaking. *Phys. Rev. X* **8**, 011016 (2018).
11. Y. Xu, H. Hu, W. Chen, P. Suo, Y. Zhang, S. Zhang, H. Xu, Phononic cavity optomechanics of atomically thin crystal in plasmonic nanocavity. *ACS Nano* **16**, 12711–12719 (2022).
12. W. Chen, P. Roelli, H. Hu, S. Verlekar, S. P. Amirtharaj, A. I. Barreda, T. J. Kippenberg, M. Kovylina, E. Verhagen, A. Martínez, C. Galland, Continuous-wave frequency upconversion with a molecular optomechanical nanocavity. *Science* **374**, 1264–1267 (2021).
13. A. Xomalis, X. Zheng, R. Chikkaraddy, Z. Koczor-Benda, E. Miele, E. Rosta, G. A. E. Vandenbosch, A. Martínez, J. J. Baumberg, Detecting mid-infrared light by molecular frequency upconversion in dual-wavelength nanoantennas. *Science* **374**, 1268–1271 (2021).
14. M. Aspelmeyer, T. J. Kippenberg, F. Marquardt, Cavity optomechanics. *Rev. Mod. Phys.* **86**, 1391–1452 (2014).
15. M. K. Dezfouli, R. Gordon, S. Hughes, Molecular optomechanics in the anharmonic cavity-QED regime using hybrid metal-dielectric cavity modes. *ACS Photonics* **6**, 1400–1408 (2019).
16. I. Shlesinger, K. G. Cognée, E. Verhagen, A. F. Koenderink, Integrated molecular optomechanics with hybrid dielectric-metallic resonators. *ACS Photonics* **8**, 3506–3516 (2021).
17. I. Shlesinger, I. M. Palstra, A. F. Koenderink, Integrated sideband-resolved sers with a dimer on a nanobeam hybrid. *Phys. Rev. Lett.* **130**, 016901 (2023).
18. S. I. Shopova, C. W. Blackledge, A. T. Rosenberger, Enhanced evanescent coupling to whispering-gallery modes due to gold nanorods grown on the microresonator surface. *Appl. Phys. B* **93**, 183–187 (2008).
19. F. De Angelis, M. Patrini, G. Das, I. Maksymov, M. Galli, L. Businaro, L. C. Andreani, E. Di Fabrizio, A hybrid plasmonic–photonic nanodevice for label-free detection of a few molecules. *Nano Lett.* **8**, 2321–2327 (2008).
20. H. M. Doeleman, E. Verhagen, A. F. Koenderink, Antenna-cavity hybrids: Matching polar opposites for Purcell enhancements at any linewidth. *ACS Photonics* **3**, 1943–1951 (2016).
21. B. Gurlek, V. Sandoghdar, D. Martín-Cano, Manipulation of quenching in nanoantenna-emitter systems enabled by external detuned cavities: A path to enhance strong-coupling. *ACS Photonics* **5**, 456–461 (2018).
22. M. K. Dezfouli, R. Gordon, S. Hughes, Modal theory of modified spontaneous emission of a quantum emitter in a hybrid plasmonic photonic-crystal cavity system. *Phys. Rev. A* **95**, 013846 (2017).
23. G. P. Acuna, F. M. Möller, P. Holzmeister, S. Beater, B. Lalkens, P. Tinnefeld, Fluorescence enhancement at docking sites of DNA-directed self-assembled nanoantennas. *Science* **338**, 506–510 (2012).
24. J. J. Baumberg, J. Aizpurua, M. H. Mikkelsen, D. R. Smith, Extreme nanophotonics from ultrathin metallic gaps. *Nat. Mater.* **18**, 668–678 (2019).
25. A. Xomalis, R. Chikkaraddy, E. Oksenberg, I. Shlesinger, J. Huang, E. C. Garnett, A. F. Koenderink, J. J. Baumberg, Controlling optically driven atomic migration using crystal-facet control in plasmonic nanocavities. *ACS Nano* **14**, 10562–10568 (2020).
26. R. J. Barbour, P. A. Dalgarno, A. Curran, K. M. Nowak, H. J. Baker, D. R. Hall, N. G. Stoltz, P. M. Petroff, R. J. Warburton, A tunable microcavity. *J. Appl. Phys.* **110**, 053107 (2011).
27. A. Moreau, C. Ciracì, J. J. Mock, R. T. Hill, Q. Wang, B. J. Wiley, A. Chilkoti, D. R. Smith, Controlled-reflectance surfaces with film-coupled colloidal nanoantennas. *Nature* **492**, 86–89 (2012).
28. H. Kelkar, D. Wang, D. Martín-Cano, B. Hoffmann, S. Christiansen, S. Götzinger, V. Sandoghdar, Sensing nanoparticles with a cantilever-based scannable optical cavity of low finesse and sub-λ^3 volume. *Phys. Rev. Appl.* **4**, 054010 (2015).
29. M. Mader, J. Reichel, T. W. Hänsch, D. Hunger, A scanning cavity microscope. *Nat. Commun.* **6**, 7249 (2015).
30. J. B. Lassiter, F. McGuire, J. J. Mock, C. Ciracì, R. T. Hill, B. J. Wiley, A. Chilkoti, D. R. Smith, Plasmonic waveguide modes of film-coupled metallic nanocubes. *Nano Lett.* **13**, 5866–5872 (2013).
31. R. Chikkaraddy, X. Zheng, F. Benz, L. J. Brooks, B. De Nijs, C. Carnegie, M.-E. Kleemann, J. Mertens, R. W. Bowman, G. A. E. Vandenbosch, V. V. Moshchalkov, J. J. Baumberg, How ultranarrow gap symmetries control plasmonic nanocavity modes: From cubes to spheres in the nanoparticle-on-mirror. *ACS Photonics* **4**, 469–475 (2017).
32. W. Yan, R. Faggiani, P. Lalanne, Rigorous modal analysis of plasmonic nanoresonators. *Phys. Rev. B* **97**, 205422 (2018).
33. J. Yang, J.-P. Hugonin, P. Lalanne, Near-to-far field transformations for radiative and guided waves. *ACS Photonics* **3**, 395–402 (2016).
34. R. Chikkaraddy, J. J. Baumberg, Accessing plasmonic hotspots using nanoparticle-on-foil constructs. *ACS Photonics* **8**, 2811–2817 (2021).
35. C. Sauvan, J. P. Hugonin, I. S. Maksymov, P. Lalanne, Theory of the spontaneous optical emission of nanosize photonic and plasmon resonators. *Phys. Rev. Lett.* **110**, 237401 (2013).
36. N. Thakkar, M. T. Rea, K. C. Smith, K. D. Heylman, S. C. Quillin, K. A. Knapper, E. H. Horak, D. J. Masiello, R. H. Goldsmith, Sculpting Fano resonances to control photonic-plasmonic hybridization. *Nano Lett.* **17**, 6927–6934 (2017).
37. H. M. Doeleman, C. D. Dieleman, C. Mennes, B. Ehrler, A. F. Koenderink, Observation of cooperative Purcell enhancements in antenna-cavity hybrids. *ACS Nano* **14**, 12027–12036 (2020).
38. P. Lalanne, W. Yan, K. Vynck, C. Sauvan, J.-P. Hugonin, Light interaction with photonic and plasmonic resonances. *Laser Photon. Rev.* **12**, 1700113 (2018).
39. A. G. Primo, N. C. Carvalho, C. M. Kersul, N. C. Frateschi, G. S. Wiederhecker, T. P. M. Alegre, Quasinormal-mode perturbation theory for dissipative and dispersive optomechanics. *Phys. Rev. Lett.* **125**, 233601 (2020).

40. A. F. Koenderink, M. Kafesaki, B. C. Buchler, V. Sandoghdar, Controlling the resonance of a photonic crystal microcavity by a near-field probe. *Phys. Rev. Lett.* **95**, 153904 (2005).
41. F. Ruesink, H. M. Doeleman, R. Hendrikx, A. F. Koenderink, E. Verhagen, Perturbing open cavities: Anomalous resonance frequency shifts in a hybrid cavity-nanoantenna system. *Phys. Rev. Lett.* **115**, 203904 (2015).
42. E. Oksenberg, I. Shlesinger, A. Xomalis, A. Baldi, J. J. Baumberg, A. F. Koenderink, E. C. Garnett, Energy-resolved plasmonic chemistry in individual nanoreactors. *Nat. Nanotechnol.* **16**, 1378–1385 (2021).
43. D. Hunger, T. Steinmetz, Y. Colombe, C. Deutsch, T. W. Hänsch, J. Reichel, A fiber Fabry-Perot cavity with high finesse. *New J. Phys.* **12**, 065038 (2010).
44. J. Mertens, M.-E. Kleemann, R. Chikkaraddy, P. Narang, J. J. Baumberg, How light is emitted by plasmonic metals. *Nano Lett.* **17**, 2568–2574 (2017).
45. P. Roelli, D. Martin-Cano, T. J. Kippenberg, C. Galland, Molecular platform for frequency upconversion at the single-photon level. *Phys. Rev. X* **10**, 031057 (2020).
46. K. Kneipp, Y. Wang, H. Kneipp, L. T. Perelman, I. Itzkan, R. R. Dasari, M. S. Feld, Single molecule detection using surface-enhanced raman scattering (sers). *Phys. Rev. Lett.* **78**, 1667–1670 (1997).
47. L. Li, T. Hutter, U. Steiner, S. Mahajan, Single molecule SERS and detection of biomolecules with a single gold nanoparticle on a mirror junction. *Analyst* **138**, 4574–4578 (2013).
48. A. A. Clerk, F. Marquardt, K. Jacobs, Back-action evasion and squeezing of a mechanical resonator using a cavity detector. *New J. Phys.* **10**, 095010 (2008).
49. C. F. Ockeloen-Korppi, E. Damskägg, J.-M. Pirkkalainen, M. Asjad, A. A. Clerk, F. Massel, M. J. Woolley, M. A. Sillanpää, Stabilized entanglement of massive mechanical oscillators. *Nature* **556**, 478–482 (2018).
50. T. Hümmer, J. Noe, M. S. Hofmann, T. W. Hänsch, A. Högele, D. Hunger, Cavity-enhanced Raman microscopy of individual carbon nanotubes. *Nat. Commun.* **7**, 12155 (2016).
51. I. M. Palstra, H. M. Doeleman, A. F. Koenderink, Hybrid cavity-antenna systems for quantum optics outside the cryostat? *Nanophotonics* **8**, 1513–1531 (2019).
52. Y. Zhang, J. Aizpurua, R. Esteban, Optomechanical collective effects in surface-enhanced Raman scattering from many molecules. *ACS Photonics* **7**, 1676–1688 (2020).

Acknowledgments: We thank I. Palstra, B. Ferrando, K. Cognée, and S. Rodriguez for fruitful discussions. **Funding:** This work is part of the Research Program of the Netherlands Organization for Scientific Research (NWO). We acknowledge support from the European Union's Horizon 2020 research and innovation program under grant agreement nos. 829067 (FET Open THOR) and 732894 (FET Proactive HOT). **Author contributions:** Conceptualization: I. S., E.V., and A.F.K. Methodology: I.S., J.V., E.O., E.V., and A.F.K. Software: I.S. and J.V. Investigation: I. S., J.V., and E.O. Visualization: I.S., J.V., and A.F.K. Supervision: E.V. and A.F.K. Writing—original draft: I.S., J.V., E.V., and A.F.K. Writing—review and editing: I.S., E.V., and A.F.K. **Competing interests:** The authors declare that they have no competing interests. **Data and materials availability:** All data needed to evaluate the conclusions in the paper are present in the paper and/or the Supplementary Materials.

Submitted 4 July 2023
Accepted 17 November 2023
Published 20 December 2023
10.1126/sciadv.adj4637

ScienceAdvances

Hybrid cavity-antenna architecture for strong and tunable sideband-selective molecular Raman scattering enhancement

Ilan Shlesinger, Jente Vandersmissen, Eitan Oksenberg, Ewold Verhagen, and A. Femius Koenderink

Sci. Adv. **9** (51), eadj4637. DOI: 10.1126/sciadv.adj4637

Science Advances (ISSN 2375-2548) is published by the American Association for the Advancement of Science. 1200 New York Avenue NW, Washington, DC 20005. The title *Science Advances* is a registered trademark of AAAS.